Physics of the Earth and Planetary Interiors 182 (2010) 152–160

Contents lists available at ScienceDirect

Physics of the Earth and Planetary Interiors

journal homepage: www.elsevier.com/locate/pepi

A simple physical model for deep moonquake occurrence times

R.C. Weber [a,*], B.G. Bills [b], C.L. Johnson [c]

[a] USGS Astrogeology Science Center, 2255 N. Gemini Drive, Flagstaff, AZ 86001, United States
[b] NASA Jet Propulsion Laboratory, Pasadena, CA, United States
[c] UBC Department of Earth and Ocean Sciences, Vancouver, BC, Canada

ARTICLE INFO

Article history:
Received 3 December 2009
Received in revised form 3 June 2010
Accepted 20 July 2010

Edited by: M. Jellinek.

Keywords:
Moon
Moonquakes
Lunar interior
Lunar seismology

ABSTRACT

The physical process that results in moonquakes is not yet fully understood. The periodic occurrence times of events from individual clusters are clearly related to tidal stress, but also exhibit departures from the temporal regularity this relationship would seem to imply. Even simplified models that capture some of the relevant physics require a large number of variables. However, a single, easily accessible variable – the time interval $I(n)$ between events – can be used to reveal behavior not readily observed using typical periodicity analyses (e.g., Fourier analyses). The delay-coordinate (DC) map, a particularly revealing way to display data from a time series, is a map of successive intervals: $I(n+1)$ plotted vs. $I(n)$. We use a DC approach to characterize the dynamics of moonquake occurrence.

Moonquake-like DC maps can be reproduced by combining sequences of synthetic events that occur with variable probability at tidal periods. Though this model gives a good description of what happens, it has little physical content, thus providing only little insight into why moonquakes occur. We investigate a more mechanistic model.

In this study, we present a series of simple models of deep moonquake occurrence, with consideration of both tidal stress and stress drop during events. We first examine the behavior of inter-event times in a delay-coordinate context, and then examine the output, in that context, of a sequence of simple models of tidal forcing and stress relief. We find, as might be expected, that the stress relieved by moonquakes influences their occurrence times. Our models may also provide an explanation for the opposite-polarity events observed at some clusters.

Published by Elsevier B.V.

1. Introduction

During Apollo missions 12, 14, 15, and 16 (1969–1972), a network of seismometers was installed on the lunar surface. Each seismic station operated continuously from inception until data collection stopped in late 1977. During that time, the network detected over 13,000 seismic events, approximately half of which are deep moonquakes (Nakamura et al., 1981).

Deep moonquakes occur between approximately 700 and 1200 km depth, roughly halfway to the center of the Moon, and originate at discrete source regions referred to as numbered "clusters" (Fig. 1). Among their unique characteristics is their tendency to occur with monthly periodicity (Ewing et al., 1971; Lammlein et al., 1974; Lammlein, 1977; Bulow et al., 2007), leading many previous investigators to address the relationship between deep moonquake occurrence and tidal stresses and strains within the Moon (Toksöz et al., 1977; Lammlein, 1977; Cheng and Toksöz, 1978; Nakamura, 1978; Goulty, 1979; Minshull and Goulty, 1988; Weber et al., 2009). Still, the physical process that results in moonquakes is not yet fully understood. Even simplified models that capture some of the relevant physics require a large number of variables. However, a single, easily accessible variable – the time interval $I(n)$ between two successive, observed events – can be used to reveal behavior not readily observed using typical periodicity analyses (e.g., Fourier analyses).

Fourier transforms of deep moonquake occurrence time histograms (number of events per day) reveal peaks at monthly and fortnightly tidal periods, in addition to peaks at longer periods (e.g., Lammlein, 1977, Fig. 2; Bulow et al., 2007, Fig. 2). More recent studies reveal refined structure in the spectra (e.g., Bulow et al., 2007, Fig. 3), indicating sensitivity to closely spaced tidal periods. The periodic behavior of deep moonquakes can also be investigated in the time domain. For example, Lammlein et al. (1974) observed that histograms of the number of deep moonquakes per day display two peaks in seismic activity each nodical month (27.21 days).

Both methods of analyzing moonquake occurrence indicate some level of periodic behavior. Additional occurrence behavior can be explored in the time domain through application of the delay-coordinate (DC) map, often used to investigate the periodic or quasi-periodic behavior of dynamical systems. DC maps (a plot of successive intervals between events: $I(n+1)$ vs. $I(n)$) provide a

* Corresponding author. Tel.: +1 928 556 7143.
E-mail address: rweber@usgs.gov (R.C. Weber).

0031-9201/$ – see front matter. Published by Elsevier B.V.
doi:10.1016/j.pepi.2010.07.009

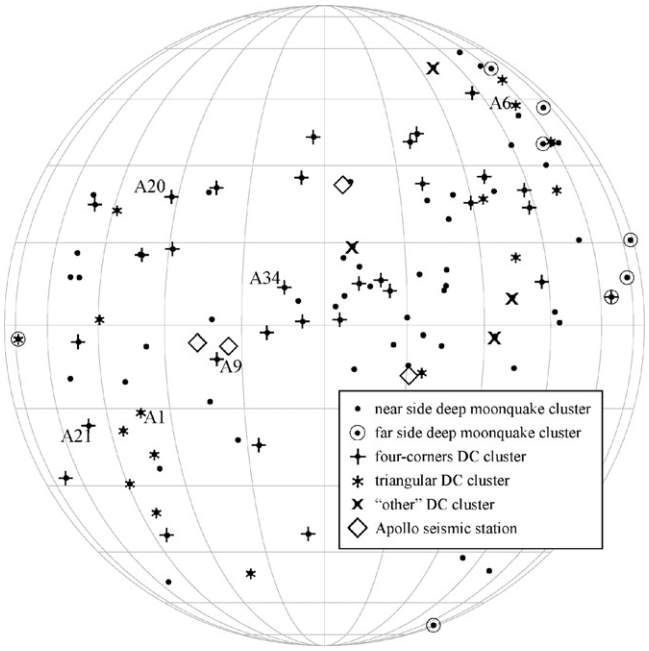

Fig. 1. Map of the Moon (15° latitude/longitude increments) showing the epicenter locations of the 98 near side and eight far side clusters identified in Nakamura (2005). The 51 clusters analyzed this study are marked according to the type of delay-coordinate behavior they exhibit. Seismic stations are, from West, Apollo 12, 14, 15, and 16.

graphical means to reveal nonlinear structure and hidden periodicities not readily discernible in the time domain. As we discuss in Section 2, Koyama (2005) first presented the application of these maps to deep moonquake occurrence data, and employed a simple statistical model (Faure et al., 2000) to account for the observed behavior. While this exercise is instructive, statistics alone do not allow for interpretation of the underlying physical cause of periodic moonquake behavior.

In this paper, we use a DC approach to characterize the mechanics of moonquake occurrence. In Sections 3 and 4, we present a simple model of stress build-up and release, from which it is possible to produce time series with DC maps resembling those of deep moonquakes. In addition, we discuss real properties of the Moon that may account for the various components of this physical model. In Section 5, we discuss the role of event polarity in our model. Lastly, in Section 6 we present a discussion of our results and conclusions.

2. A statistical model for deep moonquake periodicity

Delay-coordinate maps of discrete data are constructed by plotting the interval between two successive events $I(n+1)$ against the previous interval $I(n)$. If the intervals between events are different lengths, the points on the map fall in different places. Several examples of DC maps of the occurrence times of deep moonquakes are shown in Fig. 2.

Nearly all clusters exhibit either the "triangular" (A1 and A6) or "four-corners" (A9 and A21) periodic behavior (Table 1). Among the 51 known clusters with at least 35 events, 16 exhibit the triangular pattern, 18 exhibit the four-corners pattern, 11 exhibit the "one-corner" pattern (a sub-category of the four-corners case, which is discussed in Section 5), four exhibit generally "boxy" but indeterminate patterns, and two exhibit special cases of the four-corners pattern. Note that we chose to analyze only those clusters with at least 35 events since clusters possessing fewer events produce poorly populated (and hence difficult to analyze) delay-coordinate maps. Overall, 41% of analyzed deep moonquake events occur in clusters that fall into the four-corners category, while 54% fall into the triangular category.

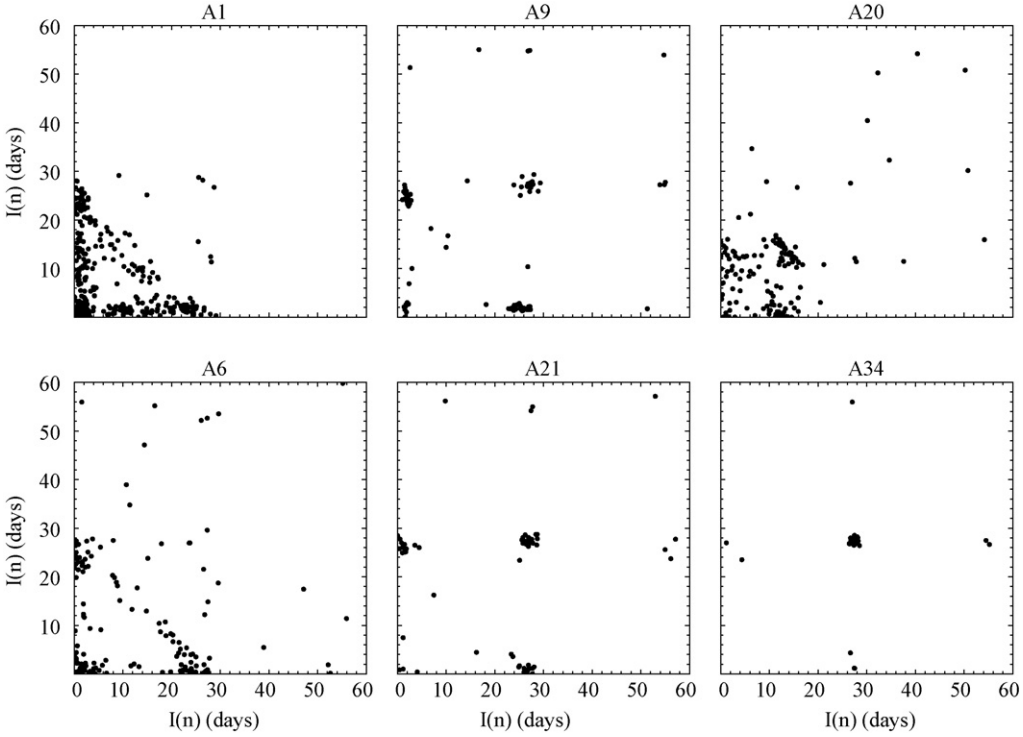

Fig. 2. Delay-coordinate maps of moonquake times from several clusters (see map in Fig. 1), illustrating two types of observed periodic behavior, which we term "triangular" (left panel), and "four-corners" (middle panel). Nearly all moonquake clusters exhibit one of these two types of periodic patterns (see text for description). The right panel shows two examples of less common pattern variations: A20 displays the four-corners pattern with events occurring twice as frequently as most clusters, while A34 displays the one-cornered pattern (a variant of the four-corners case). See Table 1 for a summary of clusters exhibiting each type of behavior.

Table 1
Summary of delay-coordinate map types among all analyzed clusters.

Delay-coordinate map type	Clusters	Number of individual events
Four-corners	A9, A15, A16, A17, A21, A22, A28, A30, A36, A38, A65, A86, A201, A202, A204, A234, A238, A257	975
One-corner (sub-category of four-corners, see Section 5)	A3, A19, A32, A33, A34, A37, A40, A41, A42, A96, A223	476
Four-corners, special case (see Section 5)	A20, A39	216
Triangular	A1, A5, A6, A7, A8, A10, A13, A14, A18, A25, A44, A51, A73, A97, A218, A224	2187
No distinct pattern	A26, A35, A100, A271	221

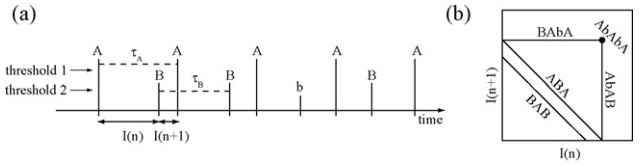

Fig. 3. (a) Time series consisting of two groups of periodic events *A* and *B*, from which the triangular pattern can be reconstructed. (b) Possible patterns that may emerge from the time series shown in (a). Lower case letters indicate events that escaped detection. At threshold 1, only *A* events are detected, so successive intervals between events group at the point labeled *AbAbA*. As the threshold is lowered, other areas of the pattern are filled in according to the labels.

If moonquakes were perfectly periodic, the interval between events would always be the same, and all data on the DC map would fall on a single point. Although Fig. 2 suggests that moonquakes are not perfectly periodic, the triangular and four-corners shapes are a consequence of certain periodicities that are present in the moonquake data.

Faure et al. (2000) proposed a simple statistical technique that shows how the triangular pattern emerges from a time series. Consider a sequence of two types of events, *A* and *B*, occurring at periods τ_A and τ_B (Fig. 3a). The *A* events result in larger amplitude signals than the *B* events. If the event detection threshold is below *A* but above *B*, then only *A* events are detected, and all points in the DC map would fall at the point shown in Fig. 3b. As the threshold in Fig. 3a is lowered to the point where *B* events are detected, the diagonals on Fig. 3b are filled in. If *A* or *B* events are of variable magnitude, then only a percentage will be detected (in Fig. 3 the events that escape detection are indicated with lower case letters), and the horizontal and vertical lines on Fig. 3b are filled out.

Koyama (2005) showed that the Faure et al. (2000) technique could be used to approximate the triangular DC map that many moonquake clusters produce, when tidal periods are chosen for τ_A and τ_B. In his model, a pair of events occur at the period of the anomalistic month (27.55 days, the time between successive perigee crossings), separated by a few days. Additionally, a second single event occurs at the period of the draconic month (27.21 days, the time between successive ascending nodal passages). Variable event magnitude is introduced by allowing events to occur with a given probability; in this case, there is a 70% chance that any given event will occur. To reproduce the observed scatter on the moonquake DC maps, Koyama's event times are drawn from a uniform random distribution over an interval ±1 day about the purely periodic times. A DC map for synthetic moonquake times created with a similar model is shown in Fig. 4a.

With slight modifications, this model can also be used to approximate the four-corners DC map. Note that both patterns can be reproduced with a time series of three monthly events occurring with some probability (~70–80% works well for moonquake-like patterns). However, unlike the triangular DC map, in the four-corners case, all three events occur at the same period (Fig. 4b).

These results support previous time domain studies and Fourier analyses, and indicate that most moonquake time series consist of groups of non-random periodic events. We next present and analyze a simple physical model of stress buildup and release, which

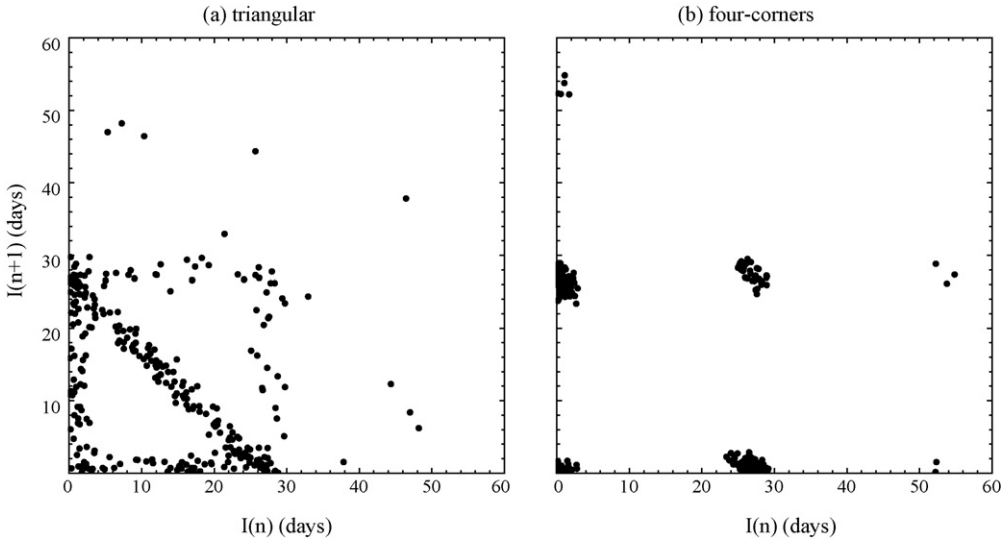

Fig. 4. Delay-coordinate map occurrence patterns that emerge from synthetic time series. (a) The triangular pattern. Two events occur at period $A = 27.55$ days, and one event occurs at period $B = 27.21$ days, all with a probability of 70% and a random uniform spread of 1 day about each of the periods *A* and *B*. For example, the first event occurs at time $t_1 + \delta t$, where t_1 is either *A* or *B*, and δt is randomly selected from the uniform interval −0.5 to 0.5 day. (b) The four-corners pattern. Three events occur with a probability of 70% at period $A = 27.55$ days, with a random uniform spread of 1 day about *A*.

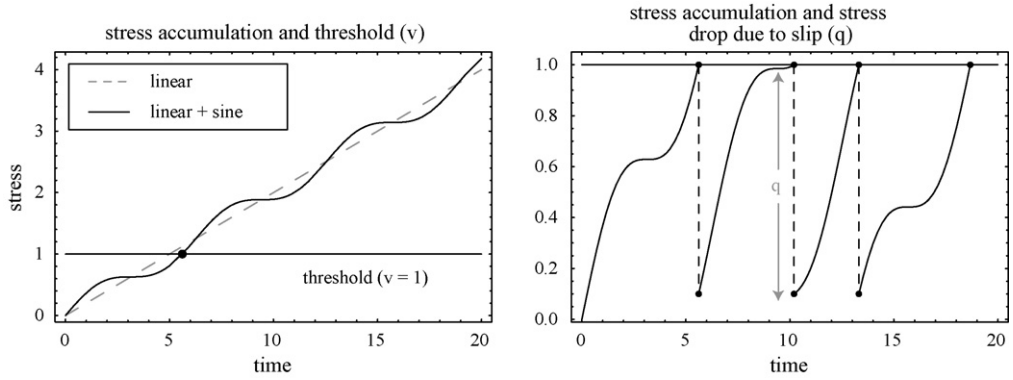

Fig. 5. Example stress accumulation and relief for background stress $S(t) = 0.2t + 0.2\sin(t)$. The threshold ν is set at a stress value of 1, and a fixed amount of the stress is relieved ($q = 0.9$) when the threshold is reached. The dots indicate the times at which the first few slip events occur.

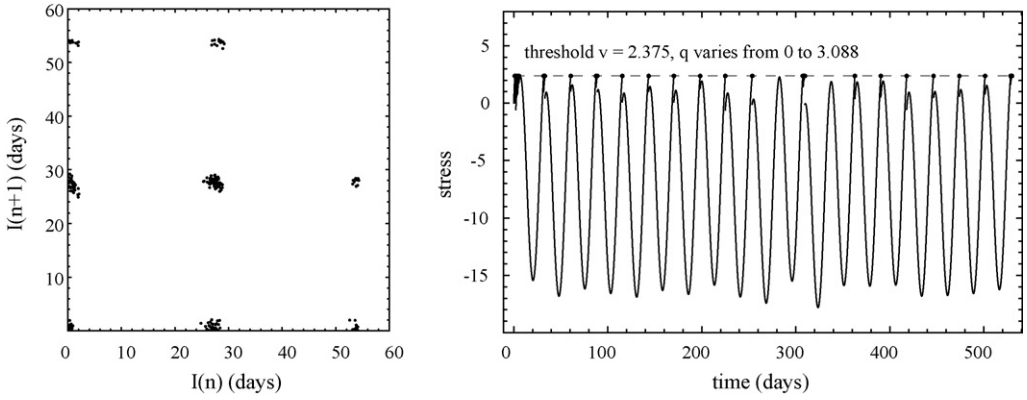

Fig. 6. Delay-coordinate map and resulting stress accumulation and relief for background stress $S(t) = 0.07t + 9.36\sin(0.228t)$. The threshold ν is set at a stress value of 2.375, and a random amount of the stress is relieved (q is a random number drawn from the uniform distribution between 0 and 3.088) when the threshold is reached.

can be used to approximate the time series necessary to produce a sequence of events whose DC maps are similar to those of moonquakes.

3. A physical model for deep moonquake periodicity

In our model, we assume the Moon is subjected to a background stress S, which is composed of two components: one that accumulates linearly with time, and one that is periodic in time:

$$S(t) = bt + c\ \sin(ft) \tag{1}$$

Note that we are not modeling a stress tensor, but simply a secular "stress" function $S(t)$ that we assume captures the relevant temporal behavior. Whenever the background stress level reaches a fixed threshold value ν, failure occurs, relieving a fixed amount q of the accumulated stress. Thus the stress at and just after each slip event is constant, but the intervals of time separating slip events are variable, since the phase of the sinusoidal oscillation at the failure threshold will vary from one event to the next.

The first slip event occurs when the stress first reaches the threshold level. Subsequent slip events occur whenever the initial stress, minus the slip-induced stress reductions, plus the newly accumulated stress reaches the threshold value again. In such a manner the model yields a series of slip times. Fig. 5 shows an example using the values $b = 0.2$, $c = 0.2$, $f = 1$, $\nu = 1$, and $q = 0.9$ in Eq. (1).

The parameters in Eq. (1) can be adjusted to produce a time series of events whose DC maps resemble those of moonquakes. Specifically, for the sinusoidal term, we use the anomalistic month, a real tidal variation to which moonquakes are known to respond

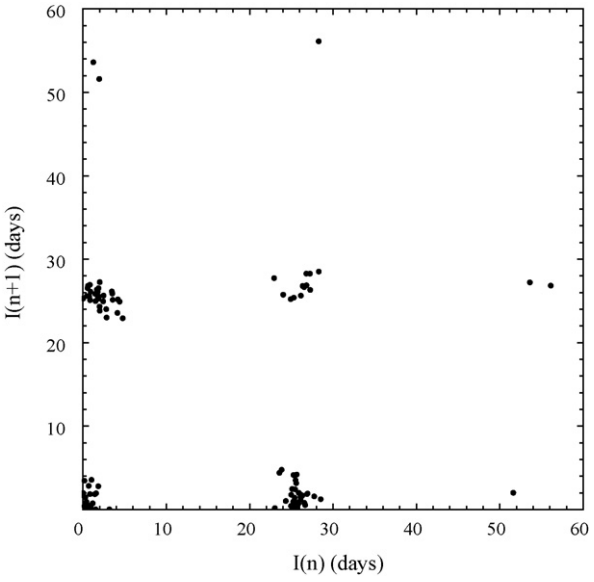

Fig. 7. Delay-coordinate map of event times computed from Eq. (2), using $a = 0$, $c_1 = 200$, $c_2 = 5$, $f_1 = 9.30 \times 10^{-4}$ ($2\pi/6758$ days or 18.6 years), and $f_2 = 0.228$ ($2\pi/27.55$ days). The threshold ν is set at a stress value of 4.0, and a random amount of the stress is relieved (q is a random number drawn from the uniform distribution between 0 and 3.6) when the threshold is reached.

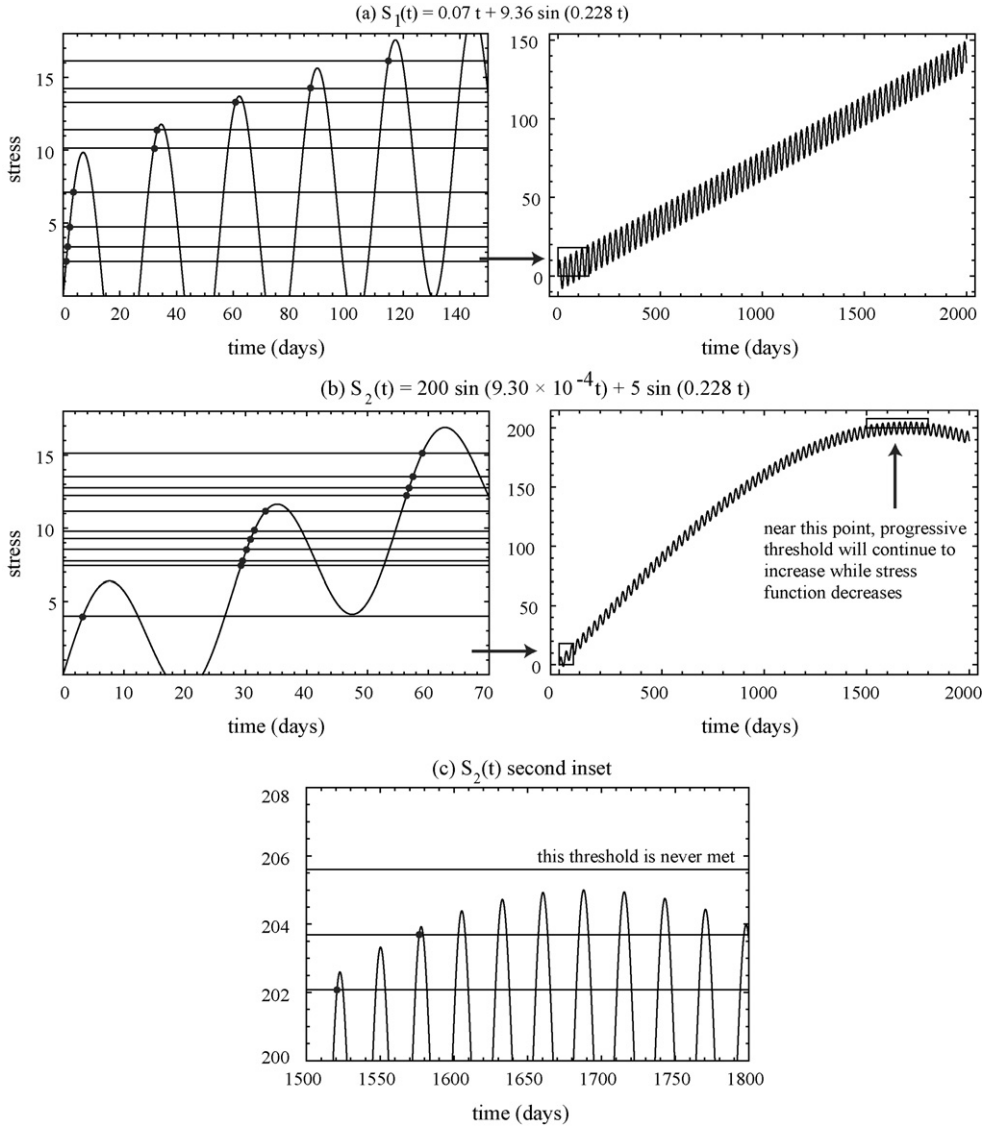

Fig. 8. Stress accumulation functions and failure thresholds for Eqs. (1) and (2). Unlike Figs. 5 and 6, the stress thresholds (horizontal lines) are plotted progressively, and stress relief is not plotted. Dots show when events occur. (a) Stress function for the DC map shown in Fig. 6, for Eq. (1) with $S_1(t) = 0.07t + 9.36\sin(0.228t)$, $\nu = 2.375$, and q varying randomly between 0 and 3.088. The plot on the left focuses on the boxed region from the plot on the right. In this example, the stress function will always increase due to the presence of the linear term, so the next threshold will always be met and events will occur indefinitely. (b) Stress function for the DC map shown in Fig. 7, for Eq. (2) with $S_2(t) = 200\sin(9.30 \times 10^{-4}t) + 5\sin(0.228t)$, $\nu = 4$, and q varying randomly between 0 and 3.6. The 18.6-year periodicity used to replace the linear term over short timescales causes the stress function to decrease after reaching maximum, meaning that events will eventually cease. (c) Second inset from (b) showing the turning point at which events cease.

(Bulow et al., 2007). Variable event magnitude is introduced by allowing the amount of stress relieved to vary between zero and q. The introduction of this random element also produces the desired scatter observed on real moonquake DC maps. Fig. 6 shows an example using the values $b = 0.07$, $c = 9.36$, $f = 0.228$ ($2\pi/27.55$ days), $\nu = 2.375$, and $q = 3.088$ in Eq. (1), resulting in the four-corners pattern. Note that the triangular pattern can not be reproduced with this model.

We conducted an exploration of values for b, c, ν, and q, and found that the DC map is very sensitive to these variables. Moonquake-like DC maps result from only a very limited range of variable values. The sensitivity to q in particular indicates that the amount of stress relieved is an important constraint on when moonquakes occur. Other models might exist that can also reproduce the observed deep moonquake occurrence patterns. However, we have chosen to focus on a specific process – tidal stress – we know to exist on and in the Moon.

3.1. Sources of the linear stress term

In the example shown above, the tidally varying sinusoidal term produces variations in stress amplitude of ~18.8 over 30 days, while the linearly increasing term produces variations in stress amplitude of ~2.1. We assume that the sinusoidally varying term is due entirely to tidal stresses in the lunar interior. Given that the tidal stresses in the deep moonquake region vary on the order of 0.1 bar over a month (see e.g., Fig. 9a and Weber et al., 2009), the linearly increasing stress term in our model should therefore increase by approximately 10 mbar per month (0.1 bar × 2.1/18.8). Various dynamic processes in the lunar interior could account for the linearly increasing term:

1. Present-day thermal convection in the lunar interior: Given Apollo observations of the lunar surface heat flow, heat transfer by Earth-like convection in the deep interior is a possibility.

However, several additional observations suggest that present-day mantle convection does not occur:

a. Age dating and crater counts have revealed that surface volcanism ended ~1.2 Gyr ago (Hiesinger et al., 2000).
b. Isotopic studies show that the lunar mare are compositionally heterogeneous (Wieczorek et al., 2006), indicating that the magmatic source regions were not homogenized by convection, and by inference suggesting that large scale mantle convection ceased prior to the production of mare basalts.
c. The Moon's radiogenic sources have been found to be concentrated largely in the crust, while the mantle is thought to be relatively depleted (Shearer et al., 2006). This suggests that the Moon loses heat by conduction rather than convection.

2. Present-day thermal contraction in the lunar interior: Thermal stresses due to differential contraction as the lunar interior cools are difficult to quantify since the rate of stress dissipation by creep is unknown. In addition, the stresses will depend on the temperature profile with depth, which is not strongly constrained by the available observations (Kuskov and Kronrod, 1998). Present-day estimates of stress due to thermal contraction performed by Solomon and Chaiken (1976) are very small, much less than 10^{-8} kbar/year (or $\sim 8.3 \times 10^{-4}$ mbar/month). This indicates that thermal contraction is also not a likely source of the linearly increasing stress term in our model.

Secular sources of stress alone are unlikely to account for the linear term in our moonquake occurrence model. However, if we assume that the lunar mantle behaves viscoelastically and can store stresses over long time periods, it may be possible that the Moon's interior is held close to a "threshold" stress level (due to the influence of some long-timescale process) that is relevant to deep moonquakes. Previous studies have similarly suggested that deep moonquakes result from an ambient background stress state to which tidal stresses are added (Toksöz et al., 1977; Minshull and Goulty, 1988). But because the deep structure of the Moon is not well-constrained, we do not feel an analysis of this effect is warranted at this time.

It may also be possible that some of the longer term variations in the lunar orbit act as the linear stress term over short time scales. These include the following:

1. Precession of the argument of periapse = 5.997 years (beat period between nodal and anomalistic months).
2. Apsidal period = 8.85 years (beat period between sidereal and anomalistic months).
3. Precession of the node, or nodal period = 18.6 years (beat period between nodal and sidereal months).

To include the second, long-period sinusoidal variation, the stress equation becomes:

$$S_2(t) = c_1 \sin(f_1 t) + c_2 \sin(f_2 t). \quad (2)$$

A DC map computed using Eq. (2) with the 18.6-year period acting as the "linear" term, and the anomalistic period as the monthly sinusoidal variation, successfully reproduces the four-corners pattern (Fig. 7). In this model, $c_1 = 200$, $c_2 = 5$, $f_1 = 9.3 \times 10^{-4}$ ($2\pi/6794$ days), $f_2 = 0.228$, $\nu = 4$, and $q = 3.6$. We note that this model requires the 18.6-year variation to be quite large compared to the monthly sinusoidal variation, while in reality the 18.6-year variation of the lunar orbit is comparatively small. Also, this model is not capable of producing events indefinitely. The stress function will eventually begin to decrease since we have replaced a perpetually increasing linear term with one that is sinusoidally varying (Fig. 8). When a local maximum is reached in the 18.6-year term of the stress function, the slip will eventually cause the stress function to decrease to the point where the threshold is no longer reached, and events cease. We know this is likely not the case for deep moonquakes, which appear to occur continuously (see e.g., Fig. 4 of Bulow et al., 2007).

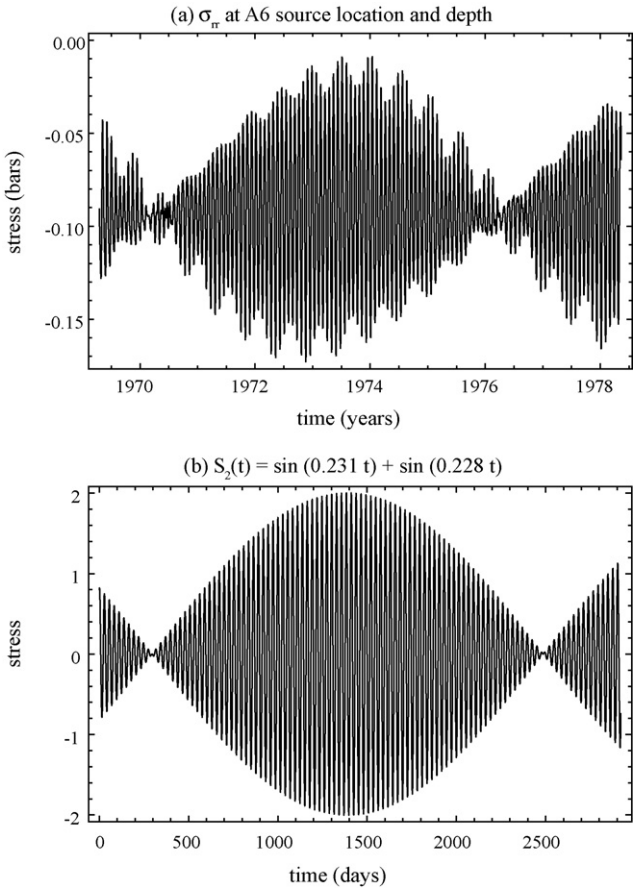

Fig. 9. (a) Radial component σ_{rr} of the tidal stress tensor computed at the A6 source location (Fig. 1) and depth (844 km) over the course of the Apollo seismic experiment. Like the stress function shown in Fig. 8b, this function is not compatible with a progressive slip model, since it begins to decrease after reaching maximum, meaning that events will eventually cease. The other components of the stress tensor display similar behavior. (b) Stress function consisting of two sinusoids with closely spaced frequencies, in this case the nodal and anomalistic months ($2\pi/27.21 = 0.231$; $2\pi/27.55 = 0.228$), plotted over a time span similar to (a).

Note that Eqs. (1) and (2) both imply progressive slip, as events occur to relieve (decrease the magnitude of) the accumulated stress implied by the linear term.

4. Revising the slip model

Although the two stress accumulation equations we have tested with our slip model result in moonquake-like DC maps, neither of them approximate the real tidal stresses resulting from the periodicities present in the lunar orbit (Fig. 9a). Tidal stress functions are not compatible with our current slip model, since a periodic (constant-mean) stress pattern will not permit perpetually increasing slip.

We revise our slip model such that periodic stress functions can be employed to produce moonquake-like DC maps. In the new slip model, Eq. (2) is still used, but now c_1 and c_2 are equal, and f_1 and f_2 are two closely spaced monthly sinusoids, such that the beat period between them produces a long-period modulation similar to that seen in the tidal stress function (Fig. 9b). In this model, $c_1 = c_2 = 1$, $f_1 = 0.231$ ($2\pi/27.21$ days), $f_2 = 0.228$, $\nu = \pm 1.6$, and $q = \pm 0.4$. Now, a fraction of the stress function is released whenever either a positive or negative threshold value is reached. If the positive threshold

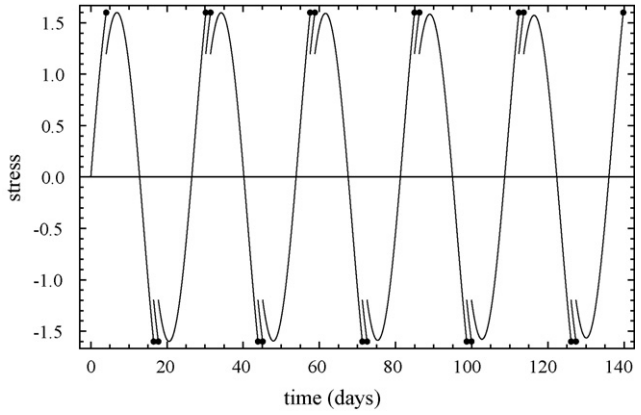

Fig. 10. Stress evolution resulting from the stress function $S_2(t) = \sin(0.231t) + \sin(0.228t)$, with $\nu = \pm 1.6$ and $q = \pm 0.4$.

is reached when the stress function is increasing, slip occurs and decreases the stress function. This is similar to the previous slip model. However, if the negative threshold is reached when the stress function is decreasing, slip occurs and increases the stress function (Fig. 10). This model implies slip-reversal, rather than progressive slip.

Initial experimentation with our revised slip model yields a four-corners pattern (Fig. 11a), but events occur approximately twice as frequently as deep moonquakes. Further modifications are necessary to adequately match real deep moonquake DC maps. We note that we have been also been unsuccessful in reproducing the triangular pattern with this revised slip model.

Slip-reversal has been suggested as a possible explanation for the opposite-polarity deep moonquakes observed at a small number of clusters (Toksöz et al., 1977; Nakamura, 2007). In the next section, we discuss how the consideration of event polarity may permit our slip-reversal model to produce moonquake-like DC maps.

5. Event polarity

In the slip-reversal example shown in Fig. 11a, let us assume that all of the events occurring at the positive threshold are of "normal" polarity, and all of the events occurring at the negative threshold are of "inverted" polarity, implying exact reversal of slip. A DC map of only the normal-polarity events is shown in Fig. 11b, and correctly reproduces the desired moonquake-like four-corners pattern.

Lammlein et al. (1974) noted that a majority of deep moonquake clusters appear to consist of events of the same polarity, implying progressive dislocation as in our previous stress model. However, they suggested that it may be possible for detectable movement in one direction to be offset by many small undetectable movements in the opposite direction. This behavior is reproducible with our slip-reversal model (Fig. 11c), and also correctly reproduces the four-corners pattern.

Nakamura (2007) identified three deep moonquake clusters possessing events of both normal and inverted polarity (A1, A20, and A25). Of these, he noted that the inverted events from A20 and A25 occur close to one-half month apart from the normal-polarity events. This behavior can be observed on a phase plot (Fig. 12a). The phase of an event is defined as the modulus of the event time with a reference period, in this case either the anomalistic or nodical month. It is thus the remainder, given in days, when an integer number of months has been subtracted from the event time. The reference month is chosen such that distinct groups of events are seen to occur at nearly opposite phases.

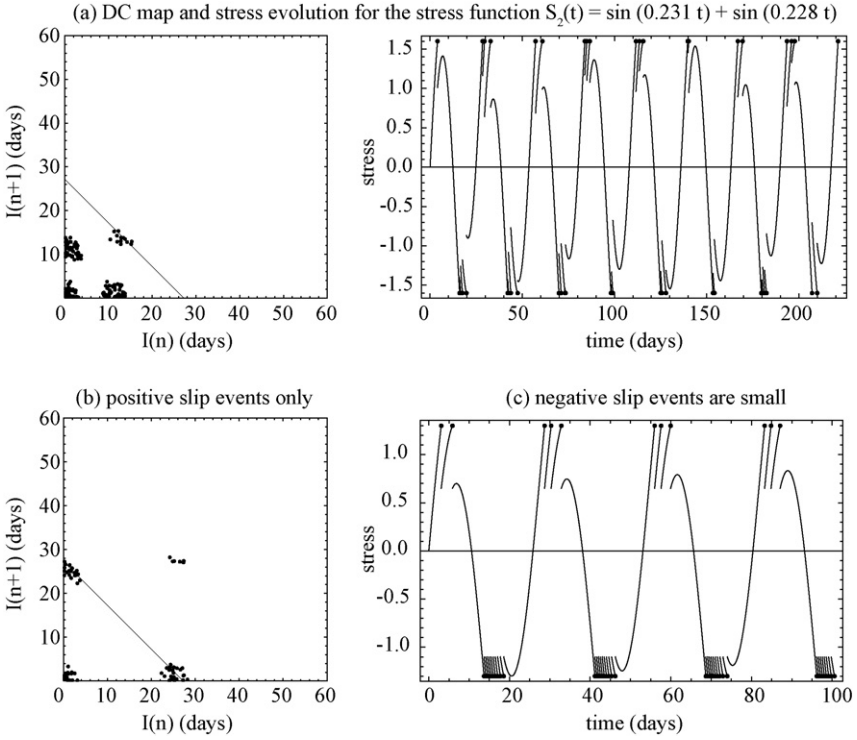

Fig. 11. (a) Delay-coordinate map and stress evolution for the stress function $S_2(t) = \sin(0.231t) + \sin(0.228t)$, with $\nu = \pm 1.6$ and q varying randomly between 0 and ± 0.6 (negative q for positive ν and vice versa). The diagonal on the DC map is aligned along the anomalistic period (27.55 days). Note that the DC map has the four-corners shape, but is too small, with events occurring approximately twice as frequently as do moonquakes. (b) DC map resulting from consideration of positive threshold events only. (c) Stress scenario in which larger positive threshold events are offset by smaller negative threshold events. In this case when the negative threshold events are disregarded (assumed to be not observed) the DC map is similar to that shown in (b).

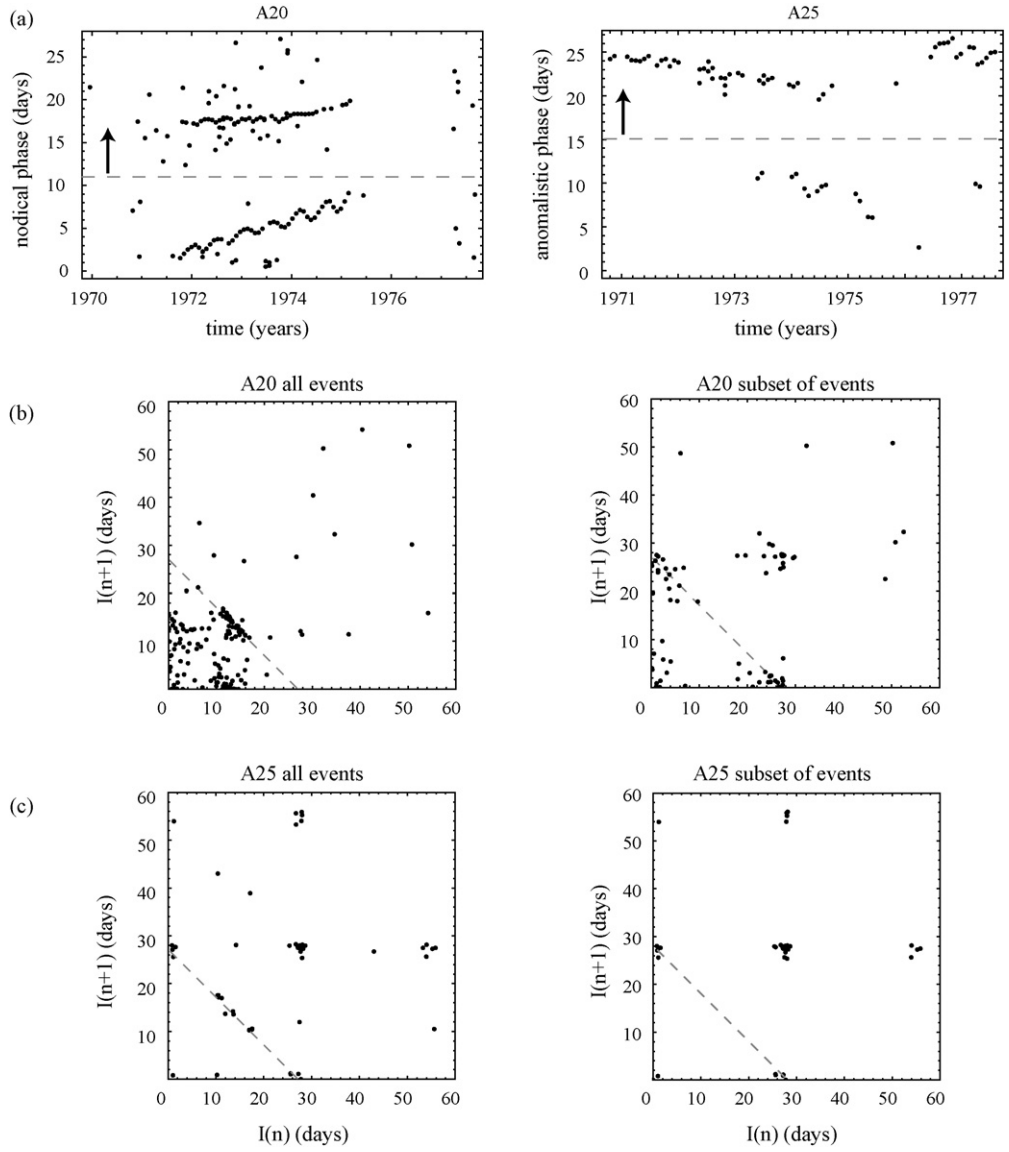

Fig. 12. (a) Nodical and anomalistic phase plots for the A20 and A25 clusters, respectively. The dotted lines mark the phase threshold used to separate events of assumed opposite polarity. (b) Delay-coordinate map of all A20 events (left) and subset of events having like polarities (right), as indicated by the arrow in (a). As in Fig. 11, the diagonal is aligned along the anomalistic period (27.55 days). (c) Same as (b) for A25.

If we assume that in both cases, all of the events falling above a certain phase threshold are of opposite polarity from those falling below said threshold, and plot DC maps of all events compared to those of only one polarity, we note the following (Fig. 12b and c):

1. For A20, the DC map for all events shows a four-corners pattern (Fig. 12b, left) that is very similar to that seen in Fig. 11a, whereas events of only one polarity show the more typical pattern (Fig. 12b, right), similar to that seen in our model (Fig. 11b).
2. For A25, neglecting events of one polarity changes a triangular DC map to a four-corners DC map (events along the diagonal are removed).

Several other clusters consist of two groups of events occurring at opposite tidal phases (and presumably of opposite polarities). Assuming that each group represents an opposite event polarity and plotting DC maps separately for each group produces similar results as for A20 and A25. A39 behaves similarly to A20, while A5, A8, and A10 behave similarly to A25. In addition, A97 and A224 change from a triangular pattern to a "one-cornered" pattern, in which the DC map shows a single group of monthly periodic events clustered near the coordinate point (27.5, 27.5). Evidently, removing assumed opposite-polarity events from certain clusters can address both of the problems of our slip-reversal stress model (too-small four-corners patterns and inability to produce triangular DC maps).

6. Discussion

With real moonquake data, the triangular pattern on the DC map emerges because the two event groups respond to different tidal months, similarly to the statistical model. This is evidenced in Fig. 12a, where the opposite-polarity A25 events fall along a slightly different slope on the phase plot. The DC map for A25 map changes to a four-corners pattern when the opposite-polarity events are ignored, but this does not explain why the opposite-polarity events respond to a different tidal month than do the normal-polarity events. In addition, not all clusters displaying the triangular pattern DC map also display distinct phase groups – in those cases there is no phase distinction between events of different polarity.

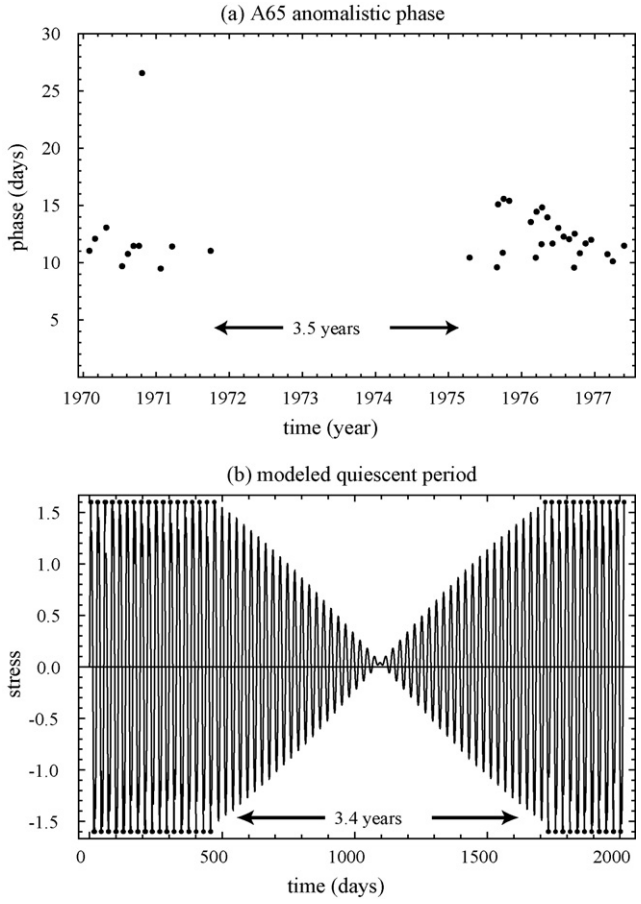

Fig. 13. (a) Anomalistic phase of A65 events. Note the approximately 3.5-year quiescent period. (b) Slip for DC map shown in Fig. 11a, displaying a similarly quiescent period.

Most of the clusters displaying the four-corners DC map also do not consist of events grouped with distinct phases. We interpret this to mean that if opposite-polarity events were produced by a given four-corners cluster (indicative of exact reversal on a pre-existing fault), they were not detected by the Apollo instruments. A possible explanation, as we suggested earlier, is that larger events in one direction could be offset by many smaller events in the opposite direction.

We note that the slip-reversal model can explain two additional properties of deep moonquake occurrence:

1. Quiescent periods: Many moonquake clusters exhibit periods of quiescence in which moonquakes temporarily cease to occur (Fig. 13a). This behavior can be reproduced with our slip-reversal model, since the 6-year beat period between the two closely spaced monthly sinusoids permits a time interval during which the stress threshold is not met (Fig. 13b).
2. Number of events: Among the 319 cataloged moonquake clusters, the average number of events per cluster detected over the 8-year span of the Apollo experiment is ~22, with the maximum being 443. The slip-reversal model predicts an average number of 77 events over a 5.5-year time span, a reasonably moonquake-like number.

7. Conclusions

We have presented two simple physical models of stress build-up and release that can reasonably account for observed deep moonquake occurrence patterns. While the first model (linear stress plus sinusoidally varying stress with progressive slip) produces moonquake-like DC maps with no manipulation, it requires a secularly increasing source of stress that is beyond the scope of our analyses to model. The second model (two closely spaced monthly sinusoids with slip-reversal) is also promising, but requires the assumption that opposite-polarity events exist but are not detected. A complete analysis of deep moonquake polarities could possibly refute this model, if clusters with four-corners DC maps are found to have opposite-polarity events. If not, we must arrive at a reasonable explanation for the lack of detection of these events by the Apollo network.

Acknowledgements

This work was supported by the Eugene M. Shoemaker Planetary Geology and Geophysics Fellowship awarded to RCW (Planetary Geology and Geophysics grant, NASA NNH08AH55I), and by a Planetary Geology and Geophysics grant, NASA NNX08AL49G, and NSERC grant to CLJ.

References

Bulow, R.C., Johnson, C.L., Bills, B.G., Shearer, P.M., 2007. Temporal and spatial properties of some deep moonquake clusters,. Journal of Geophysical Research 112, doi:10.1029/2006JE002847.
Cheng, C.H., Toksöz, M.N., 1978. Tidal stresses in the moon. Journal of Geophysical Research 83 (B2), 845–853.
Ewing, M., Latham, G., Press, F., Sutton, G., Dorman, J., Nakamura, Y., Meissner, R., Duennebier, F., Kovach, R., 1971. Seismology of the Moon and implications on internal structure, origin and evolution. In: Highlights of Astronomy. D. Reidel, pp. 155–172.
Faure, P., Kaplan, D., Korn, H., 2000. Synaptic efficacy and the transmission of complex firing patterns between neurons. Journal of Neurophysiology 84 (6), 3010–3025.
Goulty, N.R., 1979. Tidal triggering of deep moonquakes. Physics of the Earth and Planetary Interiors 19, 52–58.
Hiesinger, H., Jaumann, R., Neukam, G., Head, J.W., 2000. Ages of mare basalts on the lunar nearside. Journal of Geophysical Research 105, 29239–29276.
Koyama, J., 2005. Chaotic occurrence of some deep moonquakes. In: 36th Annual Lunar and Planetary Science Conference, (Abstract 1077).
Kuskov, O.L., Kronrod, V.A., 1998. Constitution of the Moon. 5. Constraints on composition, density, temperature, and radius of a core. Physics of the Earth and Planetary Interiors 107 (4), 285–306.
Lammlein, D.R., 1977. Lunar seismicity and tectonics. Physics of the Earth and Planetary Interiors 14 (3), 224–273.
Lammlein, D.R., Latham, G.V., Dorman, J., Nakamura, Y., Ewing, M., 1974. Lunar seismicity, structure, and tectonics. Reviews of Geophysics 12 (1), 1–21.
Minshull, T.A., Goulty, N.R., 1988. The influence of tidal stresses on deep moonquake activity. Physics of the Earth and Planetary Interiors 52, 41–55.
Nakamura, Y., 1978. A1 moonquakes: source distribution and mechanism. In: Proceedings of the 9th Lunar and Planetary Science Conference 3, pp. 3589–3607.
Nakamura, Y., 2005. Farside deep moonquakes and deep interior of the Moon. Journal of Geophysical Research 110, doi:10.1029/2004JE002332.
Nakamura, Y., 2007. Within-nest hypocenter distribution and waveform polarization of deep moonquakes and their possible implications. In: 38th Annual Lunar and Planetary Science Conference, (Abstract 1160).
Nakamura, Y., Latham, G.V., Dorman, H.J., Harris, J.E., 1981. Passive Seismic Experiment long period event catalog, revised October 2008. Tech. Rep. 118, University of Texas Institute for Geophysics.
Shearer, C.K., Hess, P.C., Wieczorek, M.A., Pritchard, M.E., Parmentier, E.M., Borg, L.E., Longhi, J., Elkins-Tanton, L.T., Neal, C.R., Antonenko, I., Canup, R.M., Halliday, A.N., Grove, T.L., Hager, B.H., Lee, D.-C., Wiechert, U., 2006. Thermal and magmatic evolution of the Moon. Reviews in Mineralogy and Geochemistry 60, 365–518.
Solomon, S.C., Chaiken, J., 1976. Thermal expansion and thermal stress in the Moon and terrestrial planets: clues to early thermal history. In: Proceedings of the 7th Lunar and Planetary Science Conference, pp. 3229–3243.
Toksöz, M.N., Goins, N.R., Cheng, C.H., 1977. Moonquakes: mechanisms and relation to tidal stresses. Science 196, 979–981.
Weber, R.C., Bills, B.G., Johnson, C.L., 2009. Constraints on deep moonquake focal mechanisms through analyses of tidal stress. Journal of Geophysical Research 114, doi:10.1029/2008JE003286.
Wieczorek, M.A., Jolliff, B.L., Khan, A., Pritchard, M.E., Weiss, B.P., Williams, J.G., Hood, L.L., Righter, K., Neal, C.R., Shearer, C.K., McCallum, I.S., Tompkins, S., Hawke, B.R., Peterson, C., Gillis, J.J., Bussey, B., 2006. The constitution and structure of the lunar interior. Reviews in Mineralogy and Geochemistry 60, 221–364.